Research Article Vol. 31, No. 12 / 5 Jun 2023 / Optics Express 18702
Optics EXPRESS

Accurate spectrogram restoration algorithm for an echelle spectrometer based on adaptive parameters

MINGJIA WANG,[1] CI SUN,[1] JIAQI CHEN,[1,2] SHULONG FENG,[1] NAN SONG,[1] ZITONG ZHAO,[1,2] JINYU WANG,[1,2] AND JIN YANG[1,*]

[1]*Changchun Institute of Optics, Fine Mechanics and Physics, Chinese Academy of Sciences, Changchun, Jilin 130033, China*
[2]*University of Chinese Academy of Sciences, Beijing 100049, China*
[*]*yang_jin1988@163.com*

Abstract: The echelle spectrometer is a high-resolution spectrometer that can realize transient direct readings of a full spectrum. To improve the accuracy of the spectrogram restoration model in calibration, multiple-integral time fusion, and an improved adaptive-threshold centroid algorithm are used to overcome noise and improve the accuracy of calculating the light spot position. A seven-parameter pyramid-traversal method is proposed to optimize the parameters of the spectrogram restoration model. The deviation of the spectrogram model is significantly reduced after the parameters are optimized, and the deviation curve fluctuation becomes mild, which greatly improves the model's accuracy after curve fitting.The test results show that the accuracy of the spot position determination algorithm proposed in this paper is 0.1 pixels. In addition to this, the accuracy of the spectral restoration model is controlled within 0.3 pixels in a short-wave stage and 0.7 pixels in a long-wave stage. Compared with the traditional algorithm, the accuracy of spectrogram restoration is more than two times, and the spectral calibration time is less than 45 min.

1. Introduction

Research on the echelle spectrometer originated more than 70 years ago [1], and early echelle spectrometers were mainly used for astrophysical plasma research [2]. The echelle spectrometer has the advantages of a wide measurement band, high spectral resolution, small volume, non-pollution, non-destructiveness, and high speed in a single exposure [3–6]. Currently, the echelle spectrometer is widely used in environmental detection, semiconductor testing, and material composition detection [7], and has become important in modern spectral analysis.

The echelle spectrometer has a cross-dispersion structure for imaging on an area array CCD. It is a major challenge to design a highly precise instrument when the light is turned many times, many optical elements are involved, the optical path is long, and the imaging surface is large. The accuracy of the echelle spectrometer is mainly affected by the following factors: 1) the deviation of the calculated spot position during spectral calibration; 2) the accuracy of the mathematical model used for ray tracing; 3) error in processing, assembly, and adjustment of optical components; 4) random detector noise; 5) the spectral drift caused by temperature changes; 6) changes in relative positions of structural parts due to stress release and instrument transportation, which lead to a change in the light path, resulting in decreased wavelength accuracy.

At present, research on calibrating the echelle spectrometer consists mainly of the following. Researchers at the Changchun Institute of Optics, Fine Mechanics and Physics have proposed a method for accurately installing and calibrating spectral instruments [8], and discussed an optical design method [9–11]. They proposed a method to improve the accuracy of the mathematical

#482021 https://doi.org/10.1364/OE.482021
Journal © 2023 Received 29 Dec 2022; revised 6 Feb 2023; accepted 6 Feb 2023; published 22 May 2023

Optics EXPRESS

model of ray tracing. To improve the accuracy of the spectrogram model, M.He proposed a method to extract the centroid of the mercury light spot quickly and effectively [12], and R. Zhang proposed using the characteristic light spot of mercury for correction [13] to overcome the influence of processing, assembly, and adjustment of parts. To solve the problem that the equipment is sensitive to temperature changes, Aya Taleb proposed a method for rapidly checking and rectifying calibration using the emission spectrum of standard laser-ablated steel [14].

Most calibration studies on echelle spectrometers have focused on optimizing the theoretical model of ray tracing [15]. In fact, factors 1, 3, 4, 5, and 6 above also have a great influence on the spectral position of the instrument. This paper first calculates the spot position with high accuracy. Then, taking the spot position as the benchmark and examining the minimum comprehensive deviation between the spectrogram model and the spot position, we obtain the real parameters of the instrument to reduce the nonlinear deviation of the spectrogram restoration model, thereby improving the calibration of the echelle spectrometer.

2. Theoretical model of the echelle spectrometer

The echelle spectrometer is a transient-measurement spectrometer that uses an echelle grating as the main dispersion element and combines it with a longitudinal dispersion element to distinguish monochromatic light of different wavelengths and different orders in two-dimensional space. Thanks to the full-wave blaze and high diffraction order of its echelle grating and core beam splitter, the echelle spectrometer simultaneously has the advantages of wide band range and high resolution. However, it is more difficult to obtain directly the wavelength of the echelle spectrometer than that of a conventional grating spectrometer. Therefore, it is necessary to establish a wavelength calibration model, that is, to establish the corresponding relationship between the detector's two-dimensional imaging coordinates and the wavelength. This process is called spectrogram restoration. The theoretical spectrogram restoration model can be obtained by geometric ray tracing according to the instrumental design parameters. The most widely used optical structure is the research object of our algorithm [16], as shown in Fig. 1.

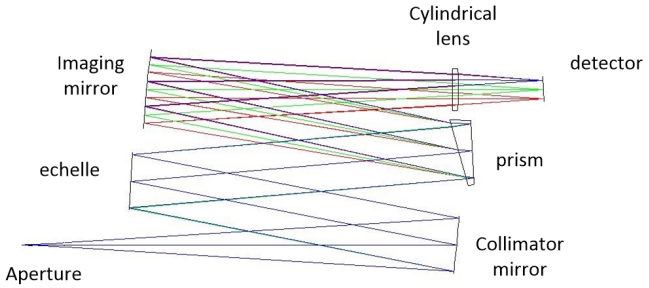

Fig. 1. Optical structure of echelle spectrometer.

The position coordinates of any wavelength on the two-dimensional image plane are jointly determined by the main dispersion element parameters, the longitudinal dispersion element parameters, and the instrumental system parameters. The relationship can be expressed as:

$$\begin{cases} DX_\lambda = f_x\left(\alpha_g, \theta, \gamma, f, \omega, \lambda\right) \\ DY_\lambda = f_y\left(\alpha_p, \beta, n_\lambda, f, \omega, \lambda\right) \end{cases} \tag{1}$$

where DX_λ is the set of position coordinates of the wavelength in the main dispersion direction, DY_λ is the set of position coordinates of the wavelength in the longitudinal dispersion direction, α_g is the incident angle of the grating, α_p is the incident angle of the prism, θ is the grating blaze

Optics EXPRESS

angle, γ is the grating offset angle, f is the focal length of the system, ω is the imaging mirror angle, β is the top angle of the prism, and n_λ is the refractive index of the prism. The coordinates (X_λ, Y_λ) of the wavelength on the detector are

$$\begin{cases} X_\lambda = \frac{DX_\lambda}{p} \\ Y_\lambda = \frac{DY_\lambda}{p} \end{cases} \tag{2}$$

where p is the detector pixel size.

Therefore, when the design parameters are known, the position of any wavelength on the detector can be obtained according to Eq. (1) and (2), and the theoretical model of the echelle spectrometer is established.

3. Accurate spectral calibration of the echelle spectrometer

In this section, the theoretical spectrogram model is matched, analyzed, and corrected using the spot position of the mercury light to complete the calibration of the echelle spectrometer. The specific contents include: accurately calculating the spot position of the mercury light spot; using triangle matching to automatically identify the corresponding characteristic spot in the mercury light image; modifying the seven model parameters α_g^*, α_p^*, θ^*, γ^*, f^*, ω^*, and β^* to build spectrogram restoration model A; calculating the residual error between the spot position and spectrogram restoration model A; fitting the residual curve on the basis of the calibrated spot position; and then constructing spectrogram restoration model B. The high-precision calibration process is shown in Fig. 2.

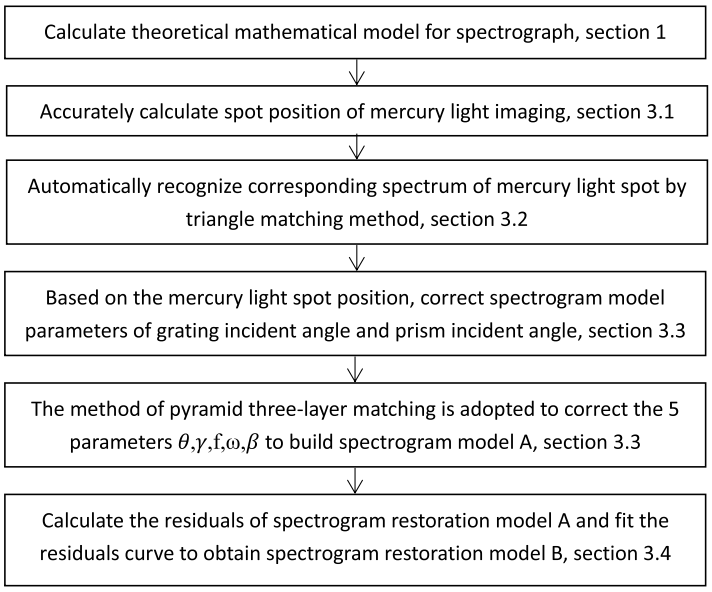

Fig. 2. High-precision spectral calibration of an echelle spectrometer.

3.1. Accurate calculation of the spot position

Calibration of the echelle spectrometer usually involves using the spot position of the element spectrum to correct the position of the theoretical model. Mercury light has many discrete characteristic peaks from 200 nm to 1000 nm, which is suitable for calibrating the instrument.

Optics EXPRESS

Precisely calculating the position of the mercury light spot is the key to ensuring a highly precise spectrogram restoration model for the echelle spectrometer. The traditional method uses local windowing and the centroid algorithm to calculate the spot position (G_x, G_y) :

$$\begin{cases} G_x = \frac{\sum_{i=U\mathrm{Up}}^{\mathrm{Down}} \sum_{j=\mathrm{Left}}^{\mathrm{Right}} x_j \times \mathrm{pixel}(i,j)}{\sum_{i=\mathrm{Up}}^{\mathrm{Down}} \sum_{j=\mathrm{Left}}^{\mathrm{Righ}} \mathrm{pixel}\ (i,j)} \\ G_y = \frac{\sum_{i=\mathrm{Up}}^{\mathrm{Down}} \sum_{j=\mathrm{Left}}^{\mathrm{Right}} y_i \times \mathrm{pixel}(i,j)}{\sum_{i=\mathrm{Up}}^{\mathrm{Down}} \sum_{j=\mathrm{Left}}^{\mathrm{Righ}} \mathrm{pixel}\ (i,j)}, \end{cases} \tag{3}$$

where $pixel(i,j)$ is the gray value of the pixel at point (i,j) in the image; x_j is the x coordinate of $pixel(i,j)$; y_i is the y coordinate of $pixel(i,j)$; and up, down, left, and right are the four boundaries of the barycentric algorithm window. However, this method is susceptible to noise, and its accuracy is difficult to guarantee.

3.1.1. Multiple-integral time fusion algorithm

The energy difference of different mercury lamps is large. For example, when overexposure occurs at a high spot energy such as at 253.652 nm, the energy of the saturated pixel is cut off and the calculated spot position is distorted. When the signal-to-noise ratio is too low at a weak spot energy such as at 794.818 nm, the background noise influences the accuracy of the spot calculation. Therefore, we adopt multiple-integral time fusion to calculate the spot position. The detector integral time is set as 2 ms, 5 ms, 10 ms, 20 ms, and 50 ms. The effectiveness of each spot is judged at these different integral times. Finally, the real positions of different spots are comprehensively calculated using the effective spot. The specific implementation is as follows:

1) We set the detector integral time p to 2 ms.

2) To reduce the influence of random noise in the image, 10 ImageRaw $_pm$ frames are collected continuously. The corresponding pixels of 10 frame images are accumulated and averaged to obtain ImageCur $_p$:

$$\mathrm{ImageCur}_p(i,j) = \sum_{m=1}^{10} \mathrm{ImageRaw}_p^m(i,j)/10 \tag{4}$$

where $\mathrm{ImageCur}_p(i,j)$ is the gray value of the composite image at position (i,j) when the integral time is p, and ImageRaw $_p$m(i,j) is the gray value of the image at position (i,j) in the m-th frame when the integral time is p.

3) At integral time p, the position of the q-th light spot is calculated, and the validity is verified according to

$$\begin{cases} Gx_p^q = \frac{\sum_{i=\mathrm{Up}}^{\mathrm{Down}} \sum_{j=\mathrm{Left}}^{\mathrm{Right}} x_j \times s_p(i,j)}{\sum_{i=Up}^{\mathrm{Down}} \sum_{j=\mathrm{Left}}^{\mathrm{Right}} s_p(i,j)} & G_{\mathrm{valid}} = 1 \quad \mathrm{MaxValue}_p^q < 65000 \,\&\, \mathrm{MaxValue}_p^q > 8000 \\ Gy_p^q = \frac{\sum_{i=\mathrm{Up}}^{\mathrm{Down}} \sum_{j=\mathrm{Left}}^{\mathrm{Right}} y_i \times s_p(i,j)}{\sum_{i=\mathrm{Up}}^{\mathrm{Down}} \sum_{j=\mathrm{Left}}^{\mathrm{Right}} s_p(i,j)}, & \\ Gx_p^q = 0, Gy_p^q = 0, & G_{\mathrm{valid}} = 0 \quad \text{else} \end{cases} \tag{5}$$

If maxvalue $_p^q$<65000 and maxvalue $_p^q$>8000, the q-th light spot at integral time p is effective; otherwise, the light spot is invalid. The maximum gray value maxvalue $_p^q$ is

$$\mathrm{MaxValue}_p^q = \max_{(i,j) \in q\ spot\ neighbor} s_p(i,j) \tag{6}$$

where $s_p(i,j)$ is the image after cut-off by adaptive threshold T_G under the integral time p. The after-cut-off image $s_p(i,j)$ is given by

$$s_p(i,j) = \begin{cases} \mathrm{ImageCur}\ (i,j) & \mathrm{ImageCur}\ (i,j) > T_G \\ 0 & \text{else} \end{cases} \tag{7}$$

Optics EXPRESS

where T_G is the adaptive threshold of the current frame image, for which the calculation method will be introduced in detail in section 3.1.2.

4) Next, we set the camera integral time p to 5 ms, 10 ms, 20 ms, and 50 ms, and repeat steps 2 and 3 to obtain the position of the q-th light spot (Gx_p^q, Gy_p^q).

5) We calculate the positions (Gx^q, Gy^q) of nine spectral calibration spots using

$$\begin{cases} Gx^q = \sum_{p=1}^{5} \mathrm{Gx}_p^q / \text{ counter}_q \\ \mathrm{Gy}^q = \sum_{p=1}^{5} \mathrm{Gy}_p^q / \text{ counter}_q \end{cases} \tag{8}$$

where counter $_q$ is the number of effective q-th light spots within the 5 integral times according to Eq. (5).

3.1.2. Calculation of the adaptive threshold T_G

The key to accurately calculating the light spot position is to select a reasonable threshold T_G. The spot calculation accuracy is reduced if T_G is too low to suppress the background noise or too high to collect all the effective pixels. The traditional method of calculating the adaptive threshold is

$$T_G = \frac{\text{peak} + \text{max}}{2} + \text{param} \tag{9}$$

where *peak* is the peak point of the histogram in the window, *max* is the brightest pixel value in the window, and *param* is an empirical parameter. As shown in Fig. 3(a), the background peak is 3204, and max is 26089. The energy difference between different mercury characteristic spectra is too large, and the empirical parameter param does not have tight constraints, so the adjustable range is too large to ensure accurate spot calculation. We combine parameters T_{Down} and T_{Up} to generate the adaptive threshold T_G. The methods of calculating T_{Down} and T_{Up} are as follows:

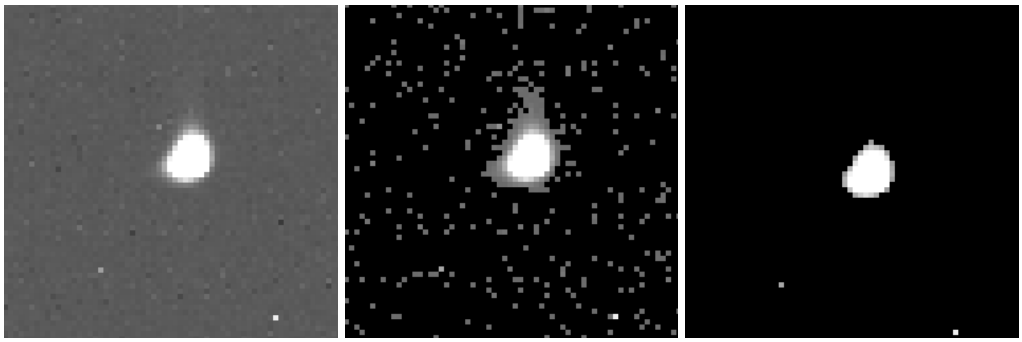

(a) Original image (b) Threshold segmentation image (c) Threshold segmentation image under

Fig. 3. Corresponding image display in the process of finding the threshold T_{Down} .

Step 1: Calculation of T_{Down}

Figure 4 shows the flow chart for calculating T_{Down} . First, we calculate the histogram peak DN_{peak} in the window, where the adjustment range of the threshold t is $(DN_{\mathrm{peak}}, 65536)$, and gradually adjust upward from DN_{peak} . During threshold segmentation, we set to 0 the pixels in window S that are lower than threshold t, and otherwise keep them unchanged. This generates a treated image image2value, as shown in Fig. 3(b). The image image2value contains a light spot and a large amount of background noise at the beginning. As threshold t increases, the independent background noise in image2value gradually decreases. The center of the light spot

Optics EXPRESS

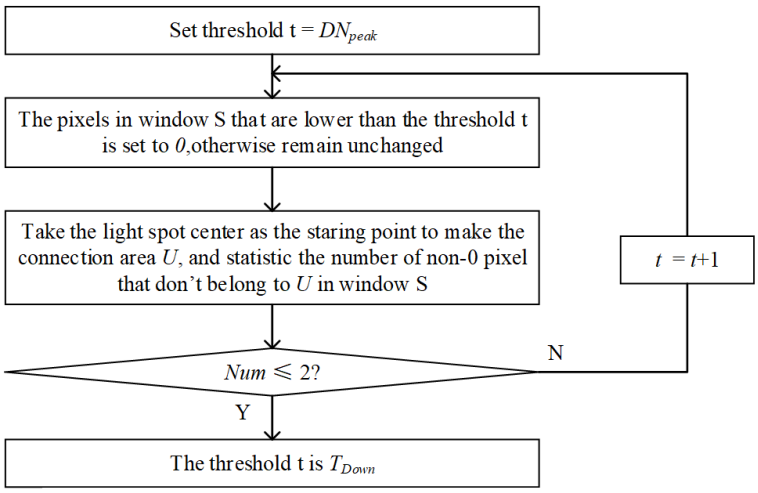

Fig. 4. Flow chart for finding T_{Down}.

is taken as the connecting area U. As shown in Fig. 3(c), when the number of non- 0 pixels in window S outside the main connecting area U is less than or equal to 2, the value of t is T_{Down} .

Step 2: Calculation of T_{Up}

The process of searching for T_{Up} is shown in Fig. 5. When the threshold t is adjusted within the background span, the fluctuation in the spot position ($\Delta x = Gx_{t+1} - Gx_t$) caused by the threshold adjustment is small because the background energy is weak relative to the spot. When the threshold t is adjusted within the light spot span, Δx tends to be large. The spot position in the x direction, Gx_t, is calculated at the threshold $t, t \in [T_{\text{Down}}, \max)$, using the Eq. (10).

$$\begin{cases} Gx_t = \dfrac{\sum_{i=\text{Up}}^{\text{Down}} \sum_{j=\text{Left}}^{\text{Right}} x_j \times s_2(i,j)}{\sum_{i=\text{Up}}^{\text{Down}} \sum_{j=\text{Left}}^{\text{Right}} s_2(i,j)} \\ s_2(i,j) = \begin{cases} f(i,j) - T_{\text{Down}} & f(i,j) > t \\ 0 & \text{else} \end{cases} \end{cases} \tag{10}$$

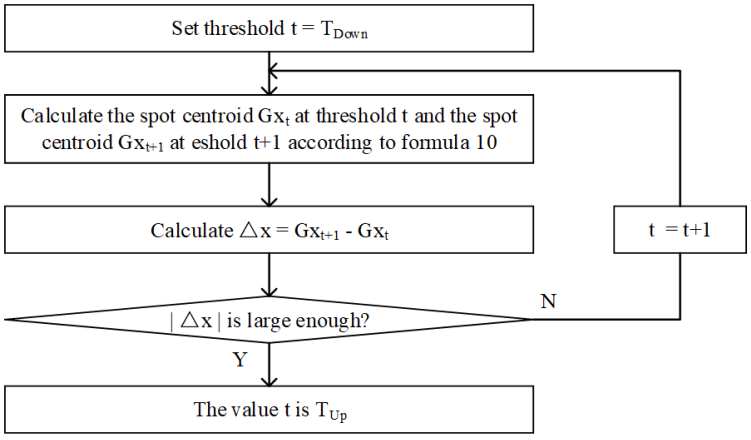

Fig. 5. Flow chart for finding T_{Up}.

Optics EXPRESS

Figure 6 shows the calculated position fluctuation of the spot in the x direction during the threshold change. The abscissa is the threshold t, the vertical coordinate is Δx, and the units are pixels. The value of T_{Up} is found through the fluctuation in the light spot centroid, and the position indicated by the red circle in Fig. 6 is T_{Up}. This means when the calculation of the light spot position generates a large fluctuation for the first time during the upward adjustment of the threshold t, the threshold t has just entered the light spot energy level from the background energy level at this time. After T_{Down} and T_{Up} are calculated, the threshold T_G for the light spot centroid can be calculated from

$$T_G = \frac{T_{\text{Down}} + T_{Up}}{2} \tag{11}$$

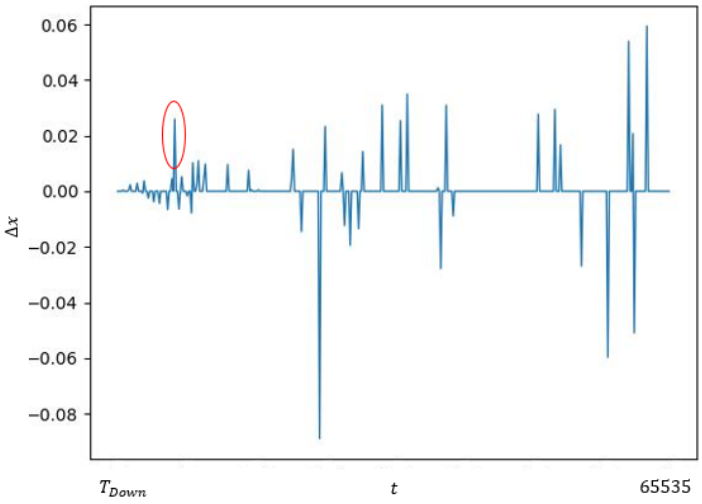

Fig. 6. Calculation of the centroid fluctuation of the light spot while threshold t changes.

3.2. *Automatic identification of the mercury light spot*

After the echelle spectrometer is installed and adjusted, there is usually a deviation between the actual position of the mercury light spot and its position in the theoretical model, and the characteristic spots of mercury light are difficult to identify. However, the relative displacement between the mercury light spot and corresponding characteristic spectrum of the theoretical model changes very little. To improve the automation of the calibration process, triangle matching is used to automatically identify the mercury light spot. Figure 7(a) shows the mercury light spot in the echelle spectrometer, Fig. 7(b) connects multiple light spots to form multiple triangles, and Fig. 7(c) shows the spatial position where the theoretical model corresponds to the detector. The four characteristic lines of the mercury light in Fig. 7(c) at 253.652 nm, 296.728 nm, 404.656 nm, and 435.833 nm are amplified to obtain Fig. 7(d).

The steps for automatic recognition of mercury light spot are as follows:

1) We calculate the internal angles $\angle BAC$, $\angle ABC$, and $\angle ACB$ of triangle $\triangle ABC$, which constitute three characteristic spectral lines of mercury at 253.652 nm, 296.728 nm, and 404.656 nm in Fig. 7(d). Let $u_0 = \angle BAC$, $v_0 = \angle ABC$, and $w_0 = \angle ACB$ in the theoretical model.

2) We calculate the positions of all mercury light spots in Fig. 7(a), and calculate the inner corners u_i, v_i, and w_i of triangle Δ_i after connecting the lines in Fig. 7(b). If triangle Δ_i satisfies any one of the following six conditions, then triangle Δ_i is similar to triangle $\triangle ABC$, and Δ_i is

Optics EXPRESS

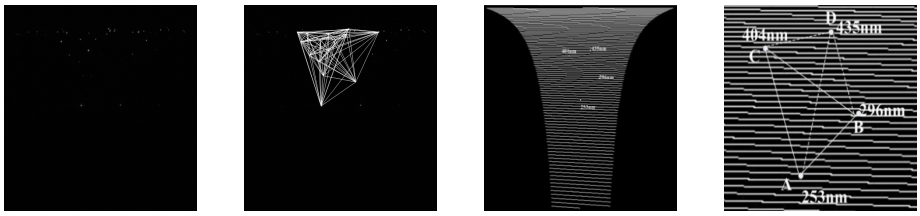

(a) Mercury light spots

(b) Multiple triangles constructed by connecting each spot in Fig. 7a

(c) Relationship between each spectrum in the theoretical model and the corresponding position in the detector

(d) Partially enlarged Fig. 7c

Fig. 7. The characteristic spectrum of the mercury light spot is automatically identified during the spectral calibration.

collected into set S_1 :

$$\begin{cases} |u_i - u_0| < 0.5^\circ \\ |v_i - v_0| < 0.5^\circ \\ |w_i - w_0| < 0.5^\circ \end{cases} \text{or} \begin{cases} |u_i - u_0| < 0.5^\circ \\ |v_i - w_0| < 0.5^\circ \\ |w_i - v_0| < 0.5^\circ \end{cases} \text{or} \begin{cases} |u_i - v_0| < 0.5^\circ \\ |v_i - u_0| < 0.5^\circ \\ |w_i - w_0| < 0.5^\circ \end{cases} \text{or}$$
$$\begin{cases} |u_i - v_0| < 0.5^\circ \\ |v_i - w_0| < 0.5^\circ \\ |w_i - u_0| < 0.5^\circ \end{cases} \text{or} \begin{cases} |u_i - w_0| < 0.5^\circ \\ |v_i - v_0| < 0.5^\circ \\ |w_i - u_0| < 0.5^\circ \end{cases} \text{or} \begin{cases} |u_i - w_0| < 0.5^\circ \\ |v_i - u_0| < 0.5^\circ \\ |w_i - v_0| < 0.5^\circ \end{cases} \tag{12}$$

3) In the theoretical model, the length of line segment AC in triangle $\triangle ABC$ is recorded as L_{AC}. Triangle Δ'_j in set S_1 is collected into set S_2 if the length of the corresponding side $L_{A'C'}$ meets the condition

$$\begin{cases} \Delta'_j \in S_2 & \text{if } (|L_{AC} - L^j_{A'C'}| < 6) \quad \Delta'_j \in S_1. \\ \Delta'_j \notin S_2 & \text{else} \end{cases} \tag{13}$$

3) Considering the fourth characteristic line at 435.833 nm in the theoretical model, we calculate $\angle BAD$ and side length L_{AD}. For each triangle Δ''_k of set S_2 with A''_k as a vertex and edge $B''_k A''_k$ as the benchmark, we rotate $\angle BAD$ to draw a straight line L'', and determine the point P'' according to the length of AD. We find the nearest mercury light spot near point P'' in Fig. 7(a) whose centroid is D''. Then, we calculate the side lengths L_{AD}, L_{BD}, and L_{CD} in Fig. 7(d) according to

$$\text{Sum}_k = \left|L_{AD} - L^k_{A''D''}\right| + \left|L_{BD} - L^k_{B''D''}\right| + \left|L_{CD} - L^k_{C''D''}\right| \tag{14}$$

and calculate the sum_k of each triangle Δ''_k in set S_2, where the triangle corresponding to minimum sum $_k$ is the result. Thus, the corresponding light spots for 253.652 nm, 296.728 nm, 404.656 nm, and 435.833 nm are determined, and spectral lines are automatically identified in Fig. 7(a).

4) In the theoretical model, we calculate $\angle CBE$ and the length of line segment BE. In Fig. 7(a), we take the 296.728 nm light spot as the vertex, and take the straight line composed of the 296.728 nm and 404.656 nm spots as the benchmark. We rotate $\angle CBE$ to draw a straight line L, determine the point E'' on the straight line L according to the length of BE, and find the nearest light spot in the neighborhood of E''. The light spot is just the point corresponding to the 576.96 nm characteristic line of mercury in the calibration image. The processes for identify the

Optics EXPRESS

mercury lines at 696.543 nm, 738.393 nm, 794.818 nm, and 912.297 nm are the same as that for 576.96 nm.

3.3. Modified spectrogram restoration model

The spectral mapping of the echelle spectrometer is affected by factors such as processing, installation, and adjustment. As shown in Fig. 8, the coordinates of the spectrum λ in the theoretical model are $S(x, y)$, and an image point of λ appears at $S'(x', y')$. Two common methods for correcting spectral deviation are the wavelength solution function and image point coordinates. The wavelength solution function solves and derives the deviation of each parameter in the function and has the advantage of fast speed, but it is too dependent on the parameters in the theoretical model, sensitive to noise, and not robust enough. The image point coordinate method usually carries out a translation transformation and scale transformation on the theoretical model to bring the spectral model closer to the actual position of the light spot [17]. Single-parameter deviation usually causes nonlinear error in the spectral restoration model, and multi-parameter deviation aliasing further increases the error complexity of this model. To reduce the influence of working-parameter deviation on the spectral calibration accuracy, we select the important parameters α_g, α_p, θ, γ, f, ω, and β for traversal, and a two-step method is adopted to reduce the computation of parameter traversal. The operations are as follows:

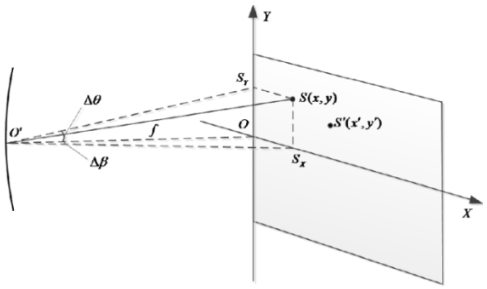

Fig. 8. Position deviation between the theoretical ray tracing model and actual spectrogram model of the echelle spectrometer.

Step 1: We optimize the grating incident angle α_g and prism incident angle α_p in the spectrogram model.

We take the spot position of mercury light as the benchmark for minimizing the comprehensive deviation between the actual spot position and the position in the spectrogram model. The grating incident angle α_g and prism incident angle α_p are traversed to complete the correction of the spectrogram model parameters, and the optimal values of α_g and α_p are obtained.

According to sections 3.1 and 3.2, we automatically identify and accurately calculate the position of the mercury light calibration spot (Gx^q, Gy^q), and α_{g0} and α_{p0} are the theoretical values of the grating and prism incidence angles. With coordinates centered on (α_{g0}, α_p), the space is traversed within a range of ±10 in the α_g and α_p directions, as shown in Fig. 9. We calculate the comprehensive deviation $\sigma^1_{(i,j)}$ between the actual position (Gx^q, Gy^q) of spot q and the position $(f_x(\alpha^i_g, \theta_0, \gamma_0, f_0, \omega_0, \lambda_q), f_y(\alpha^j_p, \beta_0, f_0, \omega_0, \lambda_q))$ at λ_q in the spectrogram model according to

$$\sigma^1_{(i,j)} = \sum_{q=1}^{9} \eta_q \times (\zeta \times (Gx^q - f_x(\alpha^i_g, \theta_0, \gamma_0, f_0, \omega_0 \lambda_q))^2 + \xi \times (Gy^q - f_y(\alpha^j_p, \beta_0, f_0, \omega_0, \lambda_q))^2) \quad (15)$$

where θ_0, γ_0, f_0, ω_0, and β_0 are the theoretical design values of parameters θ, γ, f, ω, and β; λ_q is the corresponding spectrum of the q-th calibration spot; ζ and ξ are the weight coefficients

Optics EXPRESS

assigned to the X and Y directions by the parameter correction function and should meet the condition $\zeta + \xi = 1$; and η_q is the weight coefficient of the q-th light spot and should meet the condition $\sum_{q=1}^{9} \eta_q = 9$.

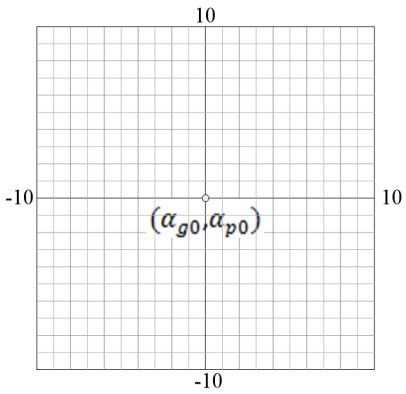

Fig. 9. Process of traversing parameters α_g and α_p.

The parameters α_g and α_p are within a ±10 traversal region. The coordinates in the traversal space (α_g^i, α_p^j) when $\sigma\ (i,j)^1$ is minimum correspond to the optimal grating incidence angle α_g^* and optimal prism incidence angle α_p^* of the spectrogram model.

Step 2: We modify the spectrogram model parameters θ, γ, f, ω, and β.

The parameters θ, γ, f, ω, and β also have a great influence on the spectrogram model. To obtain the optimal solutions of these five parameters, θ^*, γ^*, f^*, ω^*, and β^*, three-layer pyramid traversal is proposed to reduce the calculation time:

$$\sigma^2_{(i,j,k,u,v)} = \sum_{q=1}^{9} \eta_q \times (\zeta \times (Gx^q - f_x(\alpha_p^*, \theta^i, \gamma^j, f^k, \omega^u))^2 + \xi \times (Gy^q - f_y(\alpha_g^*, f^k, \omega^u, \beta^v))^2) \quad (16)$$

The three-layer pyramid-five-parameter traversal process is shown in Fig. 10. The first-layer traversal steps are θ_0, γ_0^s, f_0^s, ω_0^s, and β_0^s, and the traversal ranges are $[\theta_0 - 3\theta_0^s, \theta_0 + 3\theta_0^s]$, $[\gamma_0 - 3\gamma_0^s, \gamma_0 + 3\gamma_0^s]$, $[f_0 - 3f_0^s, f_0 + 3f_0^s]$, $[\omega_0 - 3\omega_0^s, \omega_0 + 3\omega_0^s]$, and $[\beta_0 - 3\beta_0^s, \beta_0 + 3\beta_0^s]$, respectively. When the parameters θ^i, γ^j, f^k, ω^u, and β^v are substituted into Eq. (16), the deviation σ^2 between the calibrated spot position and the position in the spectrogram model is calculated. When σ^2 is minimum, the parameters θ_1, γ_1, f_1, ω_1, and β_1 are calculated. The second-layer traversal ranges are $[\theta_1 - 3\theta_1^s, \theta_1 + 3\theta_1^s]$, $[\gamma_1 - 3\gamma^s, \gamma_1 + 3\gamma_1^s]$, $[f_1 - 3f_1, f_1 + 3f_1^s]$, $[\omega_1 - 3\omega_1^s, \omega_1 + 3\omega_1^s]$, and $[\beta_1 - 3\beta_1^s, \beta_1 + 3\beta_1^s]$. Similarly, we calculate θ_2, γ_2, f_2, ω_2, and $[\omega_2 - 3\omega^s, \omega_2 + 3\omega_2^s]$, and $[\beta_2 - 3\beta_2^s, \beta_2 + 3\beta^s]$, and we similarly calculate the optimal solutions θ^*, γ^*, f^*, ω^*, and β^*. Thus far, the optimization of the model parameters has been completed, and spectrogram model A is built according to parameters $\alpha_g^*, \alpha_p^*, \theta^*, \gamma^*, f^*, \omega^*$, and β^*.

We compare the processing time between the conventional method and the three-layer pyramid method under the same search scope and the same traversal step size. At last, we find that the processing time of the three-layer pyramid traversal method is greatly reduced. As shown in Table 1, seven parameters are decomposed into three-layer pyramid-five-parameter traversal (42 min) plus (α_g, α_p) traversal (2.8 min), which meets the required spectral calibration speed for engineering.

3.4. Position compensation in the spectrogram restoration model

After spectrogram restoration model A is constructed, there is still a certain position deviation between the calibrated spot position and the corresponding spectrum in spectrogram model A.

Optics EXPRESS

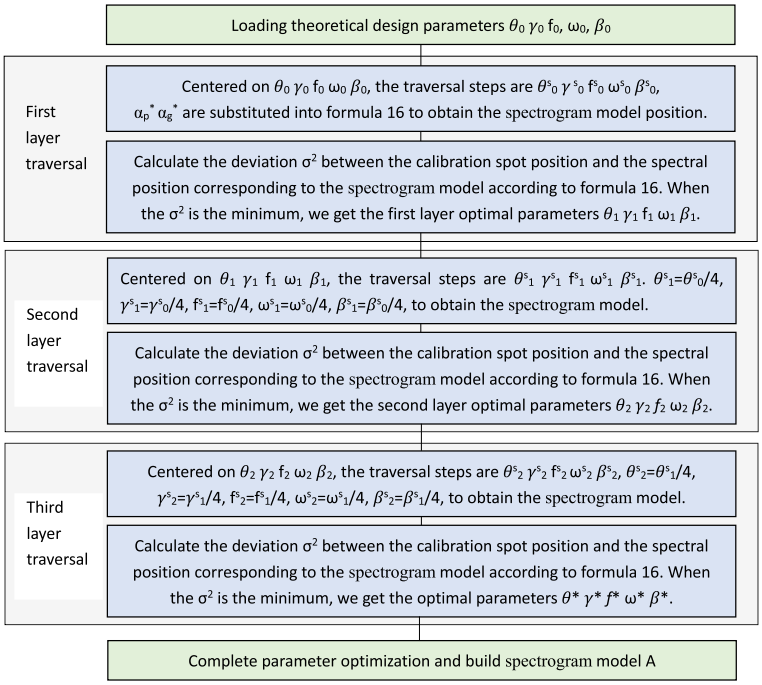

Fig. 10. Three-layer pyramid traversal process.

Next, curve fitting is used to further compensate the position in spectrogram model A, and we use a combination method of piecewise fitting and least-squares curve fitting. In the short-wave stage (200 nm–696 nm), the fluctuation in the deviation is relatively flat, so piecewise fitting is adopted to further compensate the model deviation. In the long-wave stage (696 nm–1000 nm), the fluctuation in the deviation is relatively intense, so least-squares curve fitting is used to compensate the model deviation in this stage. The deviation compensation yields spectrogram model B, which is the final spectrogram model of the echelle spectrometer.

Table 1. Comparison of processing time between conventional five-parameter traversal and three-layer pyramid-five-parameter traversal

Method	Processing time
Conventional 5-parameter traversal	19119 days
Three-layer pyramid 5-parameter traversal	42 min

4. Experiments

Accurate calculation of spot position is the key to ensure the spectrogram restoration model of high-precision echelle spectrometer. The traditional spot position calculation adopts local windowing,and the spot position deviation is 0.32 pixels. In contrast, the accuracy of spot position determination algorithm proposed in section 3.1 is 0.1 pixels, which can lay a foundation for modeling.

To verify the improved spectrogram model in this study, the spectrogram model was constructed to correspond to the echelle spectrometer, and compared with the traditional spectrogram model. The traditional approach uses the centroid method to calculate the position of the mercury light

Optics EXPRESS

spot, and uses the ray tracing method of the research group to construct the spectrogram model. The improved spectrogram model in this paper calculates the spot position according to the method in sections 3.1 and sections 3.2, similarly on the basis of the ray tracing method of the research group, and the parameter correction methods in section 3.3 are added to obtain spectrogram model A. On the basis of spectrogram model A, spectrogram model B is obtained using the position compensation in section 3.4. The nine-point calibration spectrum used to build the spectrogram model consists of 253.652 nm, 296.728 nm, 404.656 nm, 435.833 nm, 576.96 nm, 696.543 nm, 738.393 nm, 794.818 nm, and 912.297 nm, and the five test characteristic lines are 365.015 nm, 546.075 nm, 579.067 nm, 763.511 nm, and 811.531 nm. The instruments used in the experiment are shown in the Fig. 11 .The echelle spectrometer is composed of a mirror, collimator mirror, echelle, prism, imaging mirror, and detector. The design parameters of the instrument are shown in Table 2.

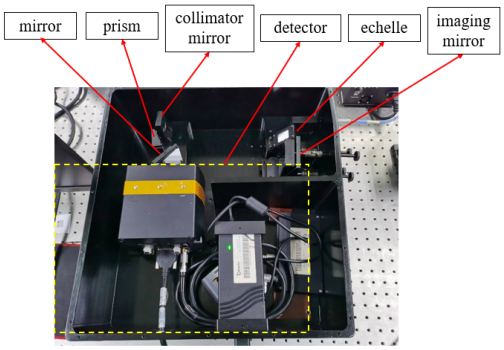

Fig. 11. Physical picture of instrument.

Table 2. Design parameters of the echelle spectrometer

Technical parameter	value
Spectral range	200–1000 nm
Spectral resolution	<0.1 nm
Focus length	300 mm
Detector	$2048 \times 2048(13.5\mu m \times 13.5\mu m)$

Figure 12 is the contrast curve of the spectral position deviation in the X direction between the actual position of 14 mercury vapor lamp characteristic spots and the traditional spectral model and the updated spectral model A in this paper, Fig. 13 is the contrast curve of the spectral position deviation in the Y direction between the actual position of 14 mercury lamp characteristic spots and the traditional spectral model and the updated spectral model A in this paper. By comparison, it is found that the deviation between the calculated spot position and the actual spot position of the updated model A is significantly reduced. On the one hand, this paper optimizes the spot extraction algorithm, the threshold is more reasonable, the anti-noise ability is improved, and the target extraction accuracy is higher. On the other hand, the 7 parameters of the spectrogram reduction model A are traced back, and the parameters of the spectrogram reduction model A are closer to the actual value of the instrument. Furthermore, the space-spectral correspondence of the spectral reduction model A is more accurate. We also found that compared with the traditional spectral reduction model, the jitter amplitude of the deviation curve in the X and Y directions of the updated model A becomes gentle with the increase of wavelength, and the gentle curve makes the spectral reduction model A more suitable for curve fitting.

Optics EXPRESS

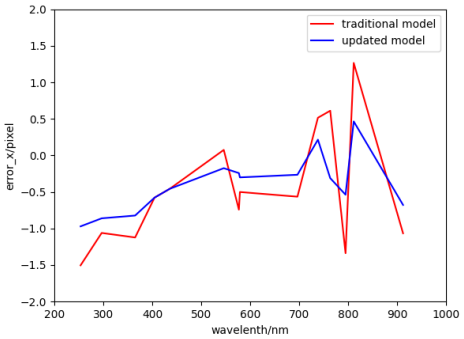

Fig. 12. Comparison of deviation in X direction between traditional model and updated model.

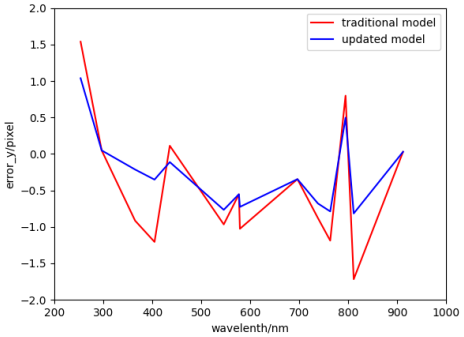

Fig. 13. Comparison of deviation in Y direction between traditional model and updated model.

Table 3. Deviation comparison between the mercury test spectrum and corresponding positions of three spectrogram models.

Number	Wavelength (nm)	Traditional pectrogram model		Spectrogram model A		Spectrogram model B	
		model x-facula x	model y-facula y	model x-facula x	model y-facula y	model x-facula x	model y-facula y
1	365.015	−1.123	−0.915	−0.824	−0.212	−0.053	−0.148
2	546.075	0.075	−0.967	−0.163	−0.746	0.113	−0.266
3	579.067	−0.501	−1.027	−0.317	−0.716	−0.079	−0.147
4	763.511	0.611	−1.189	−0.329	−0.779	−0.138	−0.498
5	811.531	1.265	−1.717	0.448	−0.810	0.638	−0.529

The traditional spectrogram model, spectrogram model A, and spectrogram model B were constructed with the nine characteristic spots of mercury light. Table 3 compares the model accuracies using the five test lines. The deviation between the traditional spectrogram model and the spot position is $[-1.717, 1.265]$, the RMSE of X direction is 0.836 and the RMSE of Y direction is 1.199; the deviation between spectrogram model A and the spot position is $[-0.824, 0.448]$, the RMSE of X direction is 0.4 and the RMSE of Y direction is 0.689; the deviation between spectrogram model B and the spot position is $[-0.529, 0.638]$, the RMSE of X direction is 0.299 and the RMSE of Y direction is 0.358. Fig. 14 shows the comparative deviation of RMSE values of different spectrogram restoration models. Obviously the accuracy of spectrogram model A is greatly improved after parameter correction. The jitter of the deviation

Optics EXPRESS

curve in Fig. 12 and Fig. 13 is gentle in the short-wave stage, which shows that the accuracy of spectrogram model B is greatly improved after curve fitting in the short-wave stage. This test verifies that the deviation of the spectrogram model at 365.015 nm, 546.075 nm, and 579.067 nm is very small, and the model deviation in the long-wave stage (763.511 nm and 811.531 nm) is also improved to a certain extent. The test results show that the accuracy of the spectral restoration model is controlled within 0.3 pixels in a short-wave stage and 0.7 pixels in a long-wave stage.

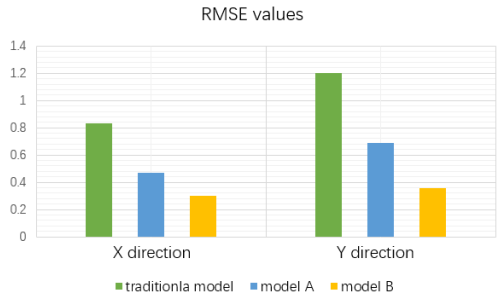

Fig. 14. Comparison of RMSE values between traditional model and updated model.

5. Conclusion

This study has enhanced the algorithmic optimization of the echelle spectrometer from two aspects. First, automatic recognition of the mercury light spot was strengthened, and the anti-interference capability was enhanced by a multi-frame accumulation algorithm and adaptive threshold algorithm, which improves the spot calculation accuracy. Second, after the model parameters were optimized, the spectrogram model was reconstructed by fitting the residual curve. By the traditional spectrogram model, the accuracy of the spectral restoration model is controlled within 1.1 pixels in a short-wave stage and 1.8 pixels in a long-wave stage. By contrast, the accuracy of the spectral restoration model is controlled within 0.3 pixels in a short-wave stage and 0.7 pixels in a long-wave stage by the spectrogram model B. An experiment comparing mercury test spectra found that spectrogram model B was significantly more accurate than the traditional spectrogram model, which verified the spectral calibration algorithm. The spectral calibration algorithm meets the engineering requirements for processing speed.

Funding. Jilin Scientific and Technological Development Program (20210204216YY); National Natural Science Foundation of China (62205333).

Disclosures. The authors declare no conflicts of interest.

Data availability. Data underlying the results presented in this paper are not publicly available at this time but may be obtained from the authors upon reasonable request.

References

1. G. R. Harrison, "The production of diffraction gratings: II. The design of echelle gratings and spectrographs," J. Opt. Soc. Am. **39**(7), 522–528 (1949).
2. D. J. Schroeder, "An echelle spectrometer-spectrograph for astronomical use," Appl. Opt. **6**(11), 1976–1980 (1967).
3. G. Ycas, F. R. Giorgetta, J. T. Friedlein, D. Herman, K. C. Cossel, E. Baumann, N. R. Newbury, and I. Coddington, "Compact mid-infrared dual-comb spectrometer for outdoor spectroscopy," Opt. Express **28**(10), 14740–14752 (2020).
4. Y. Song, A. Konar, R. Sechrist, V. P. Roy, R. Duan, J. Dziurgot, V. Policht, Y. A. Matutes, K. J. Kubarych, and J. P. Ogilvie, "Multispectral multidimensional spectrometer spanning the ultraviolet to the mid-infrared," Rev. Sci. Instrum. **90**(1), 013108 (2019).
5. D. A. Uulu, T. Ashirov, N. Polat, O. Yakar, S. Balci, and C. Kocabas, "Fourier transform plasmon resonance spectrometer using nanoslit-nanowire pair," Appl. Phys. Lett. **114**(25), 251101 (2019).
6. R. Zhang, W. Y. Ren, Z. L. Xu, H. Wang, J. G. Jiang, Y. Y. Wang, and X. B. Luo, "Single-pixel echelle spectrometer based on compressive sensing," Optik **240**, 166813 (2021).

Optics EXPRESS

7. C. Haisch and H. Becker-Ross, "An electron bombardment CCD-camera as detection system for an echelle spectrometer," Spectrochim. Acta, Part B **58**(7), 1351–1357 (2003).
8. S. J. Chen, J. C. Cui, and Y. J. Liu, "A method of precise adjustment and calibration for high-resolution echelle spectrograph, Spectroscopy and spectral analysis," **32**, 2280–2285 (2012).
9. L. Yin, Bayanheshig, J. Yang, and Y. X. Lu, "High accuracy spectral reduction algorithm for the echelle spectrometer," Appl. Opt. **55**(13), 3574–3581 (2016).
10. Rui Zhang, Bayanheshig, Lu Yin, Xiaotian Li, Jicheng Cui, Jin Yang, and Ci Sun, "Wavelength calibration model for prism-type echelle spectrometer by reversely solving prism's refractive index in real time," Appl. Opt. **55**(15), 4153–4158 (2016).
11. J. Yang, L. Yin, X. F. Yao, Bayanheshig, Y. G. Tang, and J. W. Zhu, "Optical Design and Stray Light Suppression of a New Portable Echelle Spectrometer," Acta optica sinica. **35**(8), 1–8 (2015).
12. M. He, Y. G. Tang, S. J. Tang, Bayanheshig, and J. C. Cui, "Position acquiring of signal spots in the echelle spectrograph, Spectroscopy and spectral analysis," **32**, 849–853 (2012).
13. R. Zhang, Bayanheshig, X. T. Li, and J. C. Cui, "Establishment and correction of an Echelle cross-prism spectrogram reduction model," Opt. Commun. **403**, 401–407 (2017).
14. Aya Taleb, Chao Shen, David Mory, Katarzyna Cieślik, Sven Merk, Muhammad R. Aziz, Anna Paola Caricato, Christoph Gerhard, Frédéric Pelascini, and Jörg Hermann, "Echelle spectrometer calibration by means of laser plasma," Spectrochim. Acta, Part B **178**, 106144 (2021).
15. Fajie Duan, Yuqian Qin, Xiao Fu, Ling Ma, Tingting Huang, and Cong Zhang, "Simple spectral reduction algorithm used for the echelle spectrometer," Appl. Opt. **57**(30), 8921 (2018).
16. L. Yin, *The method of spectrum data processing for echelle spectrometer*, (University of chinese academy of sciences, 2017).
17. X. Fu, *Implementation of LIBS Echelle Spectrometer and Research on Data Processing Method*, (Tianjin University, tianjin, 2018).